Some New Operational Modes and Parameters of Stress Relaxation for the Viscoelastic Characterization of Solid Polymers. I. The "Virtual Modulus" Mode

V. N. Kytopoulos, G. D. Bourkas, E. Sideridis

National Technical University of Athens, Department of Engineering Science, Section of Mechanics, 5 Heroes of Polytechnion Avenue, GR-157 73 Athens, Greece

Received 18 July 2001; accepted 13 February 2002

ABSTRACT: A new operational (functional) parameter, the so-called virtual modulus, $\bar{E}(t)$, is introduced. By this, an attempt was made for the approximation of the function of the real modulus $E(t)$, which, as known, is valid only for instantaneous loading, namely, for zero loading times. Thus, through a simple theoretical modeling and an algorithmic approach, the determination of $E(t)$, from $\bar{E}(t)$, sets sail, at the end, to the solution of a Volterra integral equation of the second type, which, in turn, sets sail to the solution of a differential equation. By the aid of numerical integration and also of some experimental evidence, it seems that this solution is valid only for loading times approximately above 0.2 s, thus obtaining, in fact, a "pseudomodulus" of relaxation. To assess the validity of this pseudomodulus, the well-known Kohlrausch–Williams–Watt (KWW) and the power-law models were used as some crude "criteria." By means of best fit, it appeared, at the first instance, that the so-calculated pseudomodulus better obeys the power-law model than it does the KWW model. This is a certain contradiction with the so-called apparent modulus, which was obtained from experiment with a finite loading time superior to 1 s. Two other criteria that were used have shown a satisfactory proof of the validity of this modeling. © 2002 Wiley Periodicals, Inc. J Appl Polym Sci 87: 121–137, 2003

Key words: poly(propylene) (PP); relaxation; modeling; viscoelastic properties; modulus

GENERAL INTRODUCTION

The fact that test data from stress relaxation can be interpreted more easily with the theory of viscoelasticity, than in the case of creep, has increased the field of application of the relaxation. Except for its significance as an experimental method, the stress relaxation as a phenomenon has also a practical significance of application in actual life when using the materials. Thus, for example, flanges of polypropylenium in different construction elements are stressed in a compressional constant strain, where a noncontrollable relaxation of stresses in the material would cause gas leaking or alteration of the required vacuum.

Isotactic polypropylene (iPP), due to its "proper" viscoelastic behavior, is one of the most suitable materials for medical utensils, like syringes, which, during their sterilization with high γ-radiation, do not lose any of their essential properties (mechanical and physical).

Additionally, for some parts of X-ray instruments, like prestressed films on stretched windows, a relevant characterization and quality control by the stress-relaxation technique is required. Apart from its practical significance, PP is important as a "model material" as it shows [together with polyethylene (PE)] a high stress-relaxation rate,[1] which can be controlled and properly combined with changes in its structure. This structure can be easily modified in various ways through a wide change in the spectrum of the crystallization degree and morphology.[2]

Therefore, with the help of such material, there have been recently developed certain "subtechniques," such as microhardness stress relaxation,[3] step-stress relaxation,[4] and variable strain-rate stress relaxation.[5] The main purpose of these and other subtechniques is the introduction of some new operational parameters for a more practical characterization of solid polymers. Some of those parameters are population rates,[6] decay time ratio,[7] internal stresses,[8] and strain-rate sensitivity index.[4] It is worthy to mention Tobolsky's[9] remarkable effort on the development of a general method of "chemiorheology," where, through the use of the parameter of "intermittent stress relaxation," he managed to observe the dynamic evolution of the "crosslinks" in connection to the time of the vulcanization process of various elastomers.

In this extended study composed of a series of three articles, we will develop and apply some new relevant operational modes with the involvement of the corresponding "operational parameters." We believe that

Correspondence to: V. N. Kytopoulous.

Journal of Applied Polymer Science, Vol. 87, 121–137 (2003)

TABLE I
Physico-chemical Properties of the PP Used

MFI (230°C/2.16 kg)	15.4
MFI (190°C/2.16 kg)	6.1
M_w	257,500
M_n	59,000
D	4.3

this new "operational way" of investigation will not only contribute to a more integrated characterization of PP's viscoelasticity, but also to a deeper research and understanding of the viscoelastic behavior of solid polymers in general.

EXPERIMENTAL

Particular knowledge of certain constructive parameters on every polymer material, other than general properties and definition, is required before the material enters the experimental stages. Some of these parameters, such as the melt-flow index, the molecular mass and weight distribution, and the heterogeneity index (M_n, M_w, D) are given in Table I. Further characteristics of the PP used can be found in ref. 10. Isotropic materials were obtained at 150°C from compression-molded sheets with a thickness of 0.30 cm. The sheets were afterward cooled at room temperature. From these sheets, dog-bone specimens were cut, which were tested in stress relaxation. The degree of crystallization was afterward estimated by using the DSC thermographs as follows: The specific melt energy, $\Delta H = 71$ J g^{-1}, was measured using a DuPont thermal analyzer and then, based on the known value of $\Delta H_c = 165$ J g^{-1} (ref. 11), which corresponds to the "ideal" crystal, the "apparent" crystallinity was calculated approximately to 43 wt %. All tests were carried out at room temperature ($\approx$ 24°C) and using an Instron-type machine.

THEORETICAL ASSUMPTIONS

Specific remarks to the relaxation modulus

Compared to the uniaxial tension, the stress-relaxation experiment appears to be more sensitive to the viscoelastic response of the material. This happens because, although the stress is being reduced, the elastic component of deformation gradually lessens and the viscoelastic one increases. In other words, the high elastic modulus of the material serves as a kind of "amplifier" for the "tracing" of the viscoelasticity. Additionally, the fact that the initial total strain can be very low—so that there is no way for plastic deformations to interfere and hide the viscoelasticity or alter the effects—corroborates the use of $E(t)$ as a parameter for the measurement of the viscoelastic response through a relaxation test.

Undoubtedly, the relaxation process is related to the basic factor of finite loading time (strain rate), which directly influences the $E(t)$ and is indirectly being influenced by the machine's quality. Therefore, Hedworth and Stowell[12] pointed out some problems deriving from the finite loading time required to stop the crossheads and the time delay existing between the actual load and its measurement. They also noted some errors caused by the halt of the crossheads during high-speed loading, where there is an instantaneous reverse movement and which, as a result, has the imposition of an initial compressive deformation on the specimen.

Although $E(t)$ is theoretically defined as the modulus arising from an instantaneous loading—that is, from a "zero" loading time—it is obvious that, due to the finite loading time, there will be a difference between this theoretical or real modulus and the actual or apparent one deriving from the experiment. Depending on the material that we use, this difference can be either big or small, and specifically for PP, the material which we used for the experiment in question, will be big due to its high relaxation rate. Consequently, one way to reduce this difference is to minimize the loading time for the given strain.

However, this procedure can fail not only due to the problems mentioned above but also to some more which Kobayashi and Ohtani noted and tried to solve.[13] Therefore, they proved that, for high-speed loading, there is a transient crosshead speed range until the achievement of the final speed. The use of slack grips (a special kind of crossheads) was a satisfactory solution for a specific high-speed (or strain-rate) limit. But, generally speaking, we can state that the standard loading time of a range of 1 s can hardly been achieved and definitely not without serious inaccuracies. Consequently, an effort should be made to find an approximate way to calculate the relaxation modulus with loading times below 1 s, something which would prove to be quite constructive and useful for the detailed characterization of the viscoelastic behavior of a strain-rate-sensitive polymer material, such as PP in our case.

General definitions

We consider the real relaxation modulus $E(t)$ as the one which is derived from the "ideal" experiment for an instantaneous loading time step "i" $\Rightarrow 0$ with the corresponding loading time t_i and we symbolize it, in general, as $i \Rightarrow 0$, $t_{i=0} = 0$. But, given that this is not practically feasible, we define as an "apparent" modulus a different relaxation modulus $\tilde{E}_i(t)$, which derives from the experimentation with finite loading time $t_{i>0} = t_i > 0$, where index i indicates the step of loading with the corresponding loading time t_i, for a constant strain ε_0. Therefore, from the above defini-

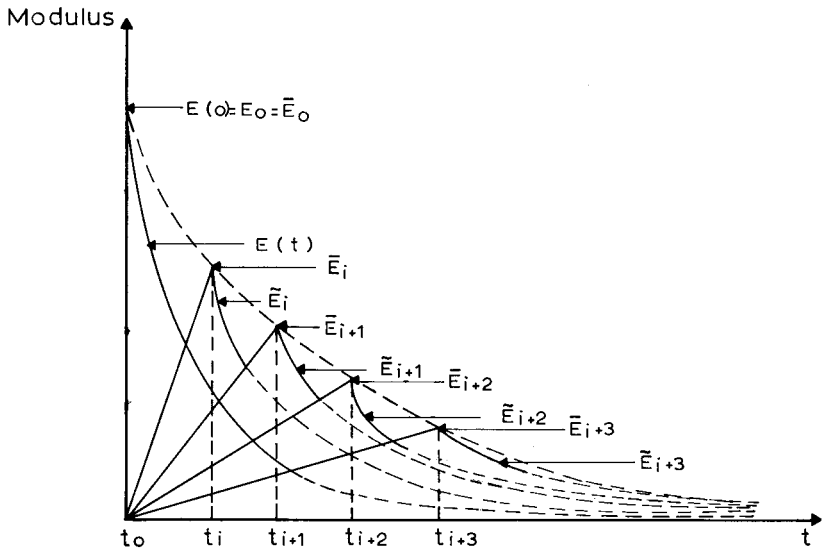

Figure 1 Schematic curves for the three types of moduli.

tions, it is concluded that $\tilde{E}_0(t) = E(t)$ for observation times $t > t_i = 0$.

Now, the achieved stress at the end of the loading time t_i and up to a certain strain ε_0 is defined by the known equation[14]

$$\sigma(t_i) = \dot{\varepsilon}_0 \int_{-\infty}^{+\infty} \tau H(1 - e^{-t_i/\tau}) d \ln \tau$$

$$= \dot{\varepsilon}_0 \int_0^{t_i} \int_{-\infty}^{+\infty} H(e^{-u/\tau}) d \ln \tau \, du \quad (1)$$

Additionally, by taking into consideration the equation

$$E(t) = \int_0^{\infty} H(\ln \tau) e^{-t/\tau} d \ln \tau \quad (1a)$$

where $H(\ln \tau)$ is the distribution spectrum (spectral density) and by combining the above two equations ($u \rightarrow t$), the result will be

$$\frac{\sigma(t_i)}{\varepsilon_0} = \frac{1}{t_i} \int_0^{\infty} E(t) \, dt = \bar{E}_i(t_i) = \text{“virtual” modulus} \quad (2)$$

This is a “new” relaxation modulus which can be expressed as a “time-averaging” of the modulus $E(t)$ and which is symbolized with a bar = average. This “new” modulus is defined as the “virtual relaxation modulus” and has, at the same time, an operational purpose in the whole procedure for the characterization of the material. In other words, the basic eq. (2) provides the stresses and the “new” moduli at the end of the loading time $t_i > 0$. Therefore, this relation represents an overlapping of a series of continuously relaxing stresses during the time interval from zero to t_i. Consequently, we have a kind of “kinematical” relaxation and not a “static” one, as it occurs in the apparent modulus (stress), where the static relaxation process evolves within the time of observation $t \geq t_i$, under fixed crossheads, that is, constant deformations. From the above, it is concluded that we can formally write $\bar{E}_i = \bar{E}_i(t_i) = \bar{E}(t)$, thus meaning that, for the virtual modulus obtained from the loading steps “i,” the loading time t_i is identical with the observation time t.

In our case, where PP is being examined, we can prove, in an original way, the validity of the following basic inequality which will be used for the theoretical modeling (see Fig. 1):

$$\bar{E}(t) > E(t) \quad (3)$$

As the procedure of proving the above is quite laborious and lengthy, the reader can refer to Appendix A. There is also the following inequality:

$$\bar{E}_i \geq \tilde{E}_i(t) \geq \tilde{E}_0(t) = E(t) \quad (4)$$

which is valid and will be used in conjuction with (3). For the same reason, the proof of this inequality is given in Appendix B. Furthermore, for loading times $t \rightarrow 0$, it must be (see Fig. 1)

$$\bar{E}_0(0) = \tilde{E}_0(0) = E(0) \quad (4a)$$

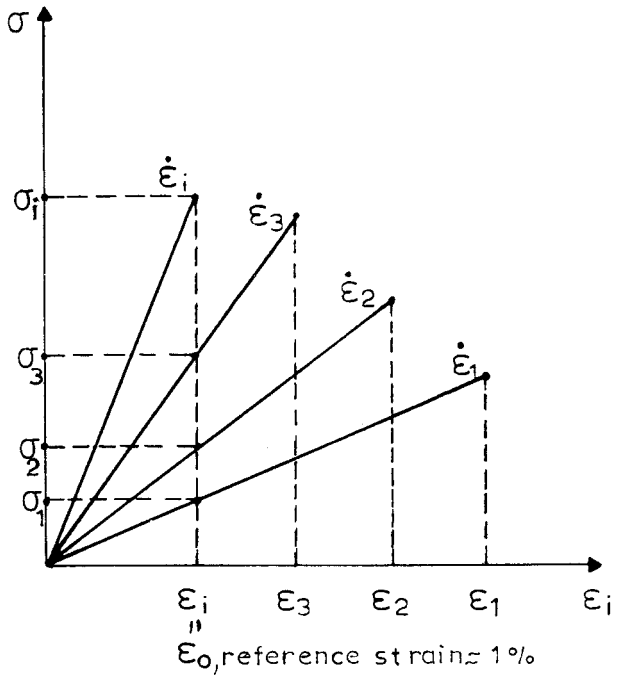

Figure 2 Loading pattern for the virtual modulus construction.

From the sketch of Figure 1, it can be seen that the virtual moduli represent the geometrical place (an envelope) of the experimental (actual) loading stresses by forming, in this sense, an "upper-limit" zone for the relaxing moduli. At the same time, the apparent modulus $\tilde{E}(t)$, which is obtained after finite loading time t_i and for observation times $t \geq t_i > 0$, must be higher than the theoretical (real) modulus $E(t)$ for the same observation time "t."

In general, for those three relaxation moduli, we can state the following: The virtual modulus $\bar{E}_i$ is obtained through a kinematic relaxation during the loading time t_i, while the apparent modulus $\tilde{E}_i(t)$ and the real modulus $E(t)$, through a static relaxation with time $t > t_i$ after finite loading time $t_i > 0$ and zero loading time $t_i = 0$, respectively.

The schematic graph in Figure 1, which explains in detail all the above, was drawn based on the aforementioned comments and the details described in Appendices A and B. Considering all the above and by experimentally measuring several $\bar{E}_i$ points, we constructed, step by step, the virtual modulus $\bar{E}(t_i)$ curve. The schematic $\bar{E}_i$ curve shown in Figure 1 was experimentally constructed from Figure 2 as follows: Several graphs of the stress/strain for different strain rates $\dot{\varepsilon}_i$ were drawn initially. The vertical abscissas were then taken, and through the horizontal ones, the corresponding stresses σ_i were drawn, for a certain prescribed reference strain ε_0 with a vertical line at ε_0. Finally, the loading time $t_i = \varepsilon_0/\dot{\varepsilon}_i$ was calculated and the diagram σ_i/ε_0 versus t_i, which presents the virtual relaxation modulus curve, was drawn.

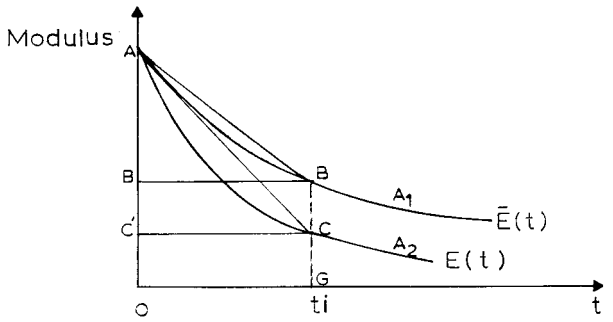

Figure 3 Schematic graph of the geometric area relations among the virtual, apparent, and real moduli.

A physical explanation of the virtual modulus can be given now, based on the aforementioned assumptions. Therefore, this modulus does not present the physical relaxation phenomenon as such and, in this sense, is not a continuously time-decay formation function in form of $E(t)$ or $\tilde{E}_i(t)$ with observation time t. On the contrary, it is a discontinuous function of loading time t_i and indicates a fictive phenomenon (fictive downward formation function versus increasing loading time).

Algorithmic approach of the real modulus by means of the virtual modulus

In the previous paragraph, it was mentioned that a material with a high strain rate sensitivity shows great differences of the apparent relaxation modulus. From the studies in ref. 5, it is known that PP has one of the highest degrees of this sensitivity and, therefore, noticeable differences of the apparent relaxation modulus for different loading times t_i are expected. To better study this problem, we tried to develop a method to approximate the real modulus $E(t)$ by the virtual modulus $\bar{E}(t)$. For this reason, some helpful data are taken from the schematic of Figure 3, where $\tilde{A}_{1,2}$ is the total "curvilinear" area between curves 1 and 2 and $A_{\triangle_1} A_{\square_{1,2}}$ are the triangular and orthogonal areas, correspondingly. The upper curve (1) represents the virtual relaxation modulus, while the lower line (2), the real one. By assuming an instantaneous loading and taking into consideration the basic inequality (3), we have

$$\tilde{A}_1 = A_{\triangle_1} + A_{\square_1}$$

$$\tilde{A}_2 = A_{\triangle_2} + A_{\square_2} \tag{5}$$

$$\tilde{A}_1 - \tilde{A}_2 = (A_{\triangle_1} - A_{\triangle_2}) + (A_{\square_1} - A_{\square_2}) > 0$$

[from inequality (3)] (6)

$$A_{\square_1} - A_{\square_2} = t[\bar{E}_i(t) - E(t)] \tag{6a}$$

$$\frac{[\bar{E}(0) - \bar{E}(t)]t}{2} = \psi_1 A_{\triangle_1}, \quad \frac{[E(0) - E(t)]t}{2} = \psi_2 A_{\triangle_2} \quad (7)$$

Also, $\psi_1(t \to 0) = 1$ and $\psi_2(t \to 0) = 1$, with $\psi_1(t) \geq 1$ and $\psi_2(t) \geq 1$. From the experiments with different loading times t_i, it was possible for the apparent modulus to obtain

$$\frac{[\tilde{E}_i(0) - \tilde{E}_i(t)]t}{2A_{\triangle_i}} = \psi_i \cong \text{const}$$

for all loading time steps $i \Rightarrow t_i$ and for the same observation times $t > t_i$ and $t \leq 3$ min. Therefore, it is valid to assume the general relation $\psi_1 \cong \psi_2 \cong \psi(t)$. This means that we do not have any influence because of the loading time, a fact that for Eqs. (7) means, in turn, an independence of the strain rate. Now, taking into consideration the basic relationships between the areas in Figure 3 and the basic relations (6), (6a) and (7), we can write

$$\tilde{A}_1 - \tilde{A}_2 = \int_0^t \bar{E}_0(t')\,dt' - \int_0^t E(t')\,dt' = \frac{t}{2\psi} \times [(\bar{E}(0) - E(0)) + E(t) - \bar{E}(t)] + t[\bar{E}(t) - E(t)] \quad (8)$$

After some algebra, we take the integral equation

$$\bar{I}(t) - \int_0^t \varphi(t')\,dt' = \frac{t}{2}\psi^{-1}(t)\varphi(t) - \frac{t}{2}\psi^{-1}(t)\chi(t) + t \cdot \chi(t) - t\varphi(t) \quad (9)$$

where

$$\bar{I}(t) = \int_0^t \bar{E}(t')\,dt', \quad \varphi(t') = \tilde{E}_0(t') = E(t'), \quad \chi(t) = \bar{E}(t)$$

and using the general assumption,

$$E(0) = \bar{E}_0(0) = \tilde{E}_0(0)$$

(at the instantaneous loading step, $i \Rightarrow t_0 = 0$, all the initial moduli are equal).

The above relation is written

$$\varphi(t)t\left[1 - \frac{1}{2\psi(t)}\right] - \int_0^t \varphi(t')\,dt' = \chi(t)t\left[1 - \frac{1}{2\psi(t)}\right] - I(t) = f(t) \quad (10)$$

This relation is a second-type Volterra integral equation and can be solved by differentiating the time variable t and obtaining the following differential equation:

$$\dot{\varphi}(t)\bar{\psi}(t) + \varphi(t)\dot{\bar{\psi}}(t) - \varphi(t) = \dot{f}(t) \quad (11)$$

or

$$\dot{\varphi}(t) + \varphi(t)\left[\frac{\dot{\bar{\psi}}(t) - 1}{\bar{\psi}(t)}\right] = \frac{\dot{f}(t)}{\bar{\psi}(t)} \quad (12)$$

and, generally,

$$\dot{\varphi}(t) + \varphi(t) \cdot P(t) = Q(t) \quad (13)$$

with

$$\bar{\psi}(t) = 1 - \frac{1}{2\psi(t)}$$

and

$$P(t) = \frac{\dot{\bar{\psi}}(t) - 1}{\bar{\psi}(t)}, \quad Q(t) = \frac{\dot{f}(t)}{\bar{\psi}(t)}$$

The above differential equation has the following closed-form general solution:

$$E(t) = \tilde{E}_0(t) = \varphi(t) = \exp\left[-\int_0^t P(t')\,dt'\right]_2\left\{\int_0^t Q(t')\exp\left[\int_0^{t'} P(x)\,dx\right] + c\right\} \quad (14)$$

where, for $t_0 = 0$, we have $c = \varphi(0) = \bar{E}_0(0) = E(0) = \tilde{E}_0(0)$.

Here, the basic fact is that, by the definition $\varphi(t) = \tilde{E}_0(t) = E(t)$, we can, theoretically at least, calculate a relaxation modulus for very short loading times, in case we know some other parameters such as c, $\chi(t)$, $\psi(t)$ and $f(t)$. Since the whole procedure of the analytical solution and the verification of the errors in the numerical integration, and also the assumptions and approximations required, are quite lengthy and time-consuming, we refer the reader to the special Appendix C. We advance here by having the results as given and will discuss them in the following section.

RESULTS AND DISCUSSION

The virtual moduli $\bar{E}_i$ points are shown in Figure 4, computed through the use of "virtual" stresses $\bar{\sigma}_i$, for various initial strains ε_0. For the points $\bar{E}_i$ for a given

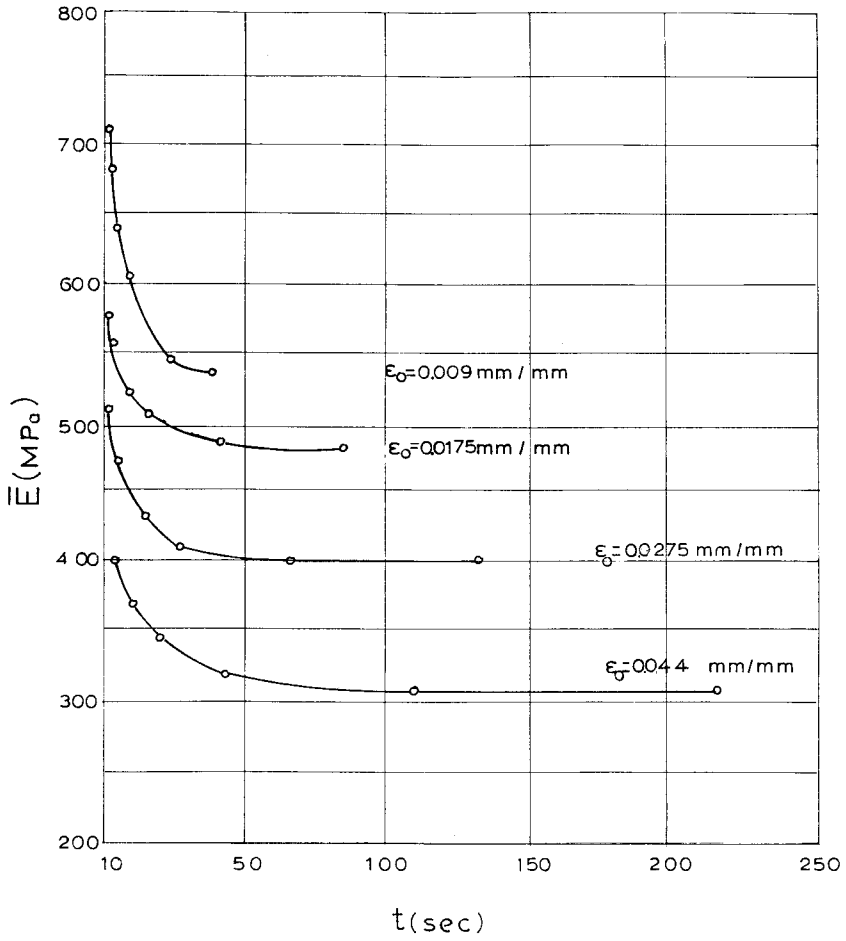

Figure 4 Experimental points of the virtual moduli curves for different reference strains ε_0.

reference $\varepsilon_0 \cong 1\%$, a "continuous" time-decay curve, shown in Figure 5, and based on the "Best-Fit" of "Jandel Table Curve 2D" software was constructed. For details, this program has been designed to fit large (8000) numbers of candidate curve-fit equations in a fully automated fashion. Among them, a "decay"

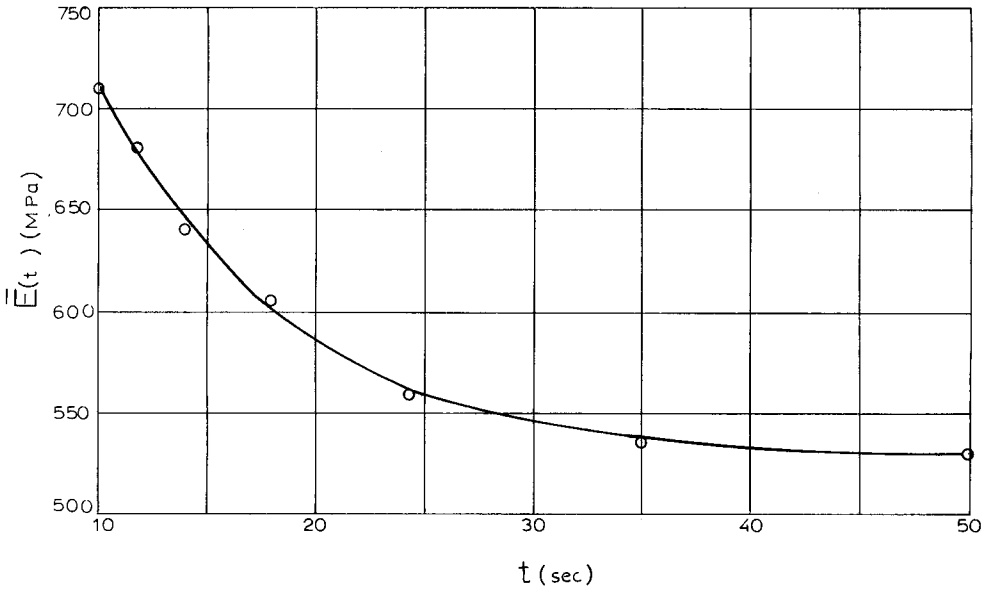

Figure 5 Construction by best-fitting procedure of a virtual modulus curve for initial reference strain $\varepsilon_0 \cong 1\%$.

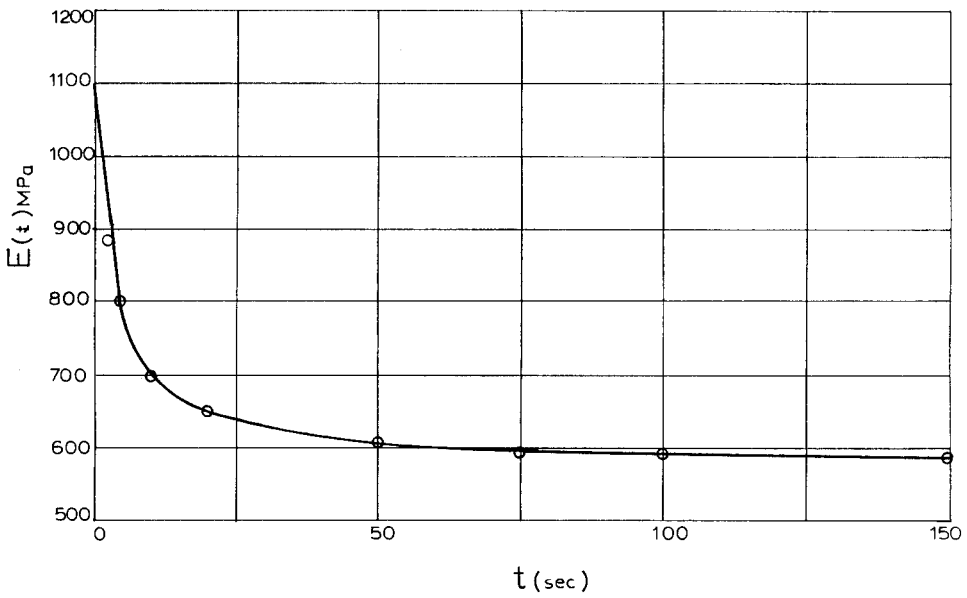

Figure 6 Calculated pseudomodulus curve by the numerical algorithms.

form function of the form $\bar{E}(t) = \bar{E}(0)e^{-a \cdot t} + \bar{E}(\infty)$ was chosen, as it was better at reflecting the relaxation phenomenon. This function, combined with a extrapolation to $t = 0$, indicatively results to $\bar{E}(0) \cong 1200$ MPa as a general, initial relaxation modulus [$\bar{E}(0) \cong \tilde{E}(0) \cong E(0)$]. Therefore, we have the constant $c = \bar{E}(0)$ in eq. (14).

The final result is shown in Figure 6, where the most suitable curve function on the $E_i(t_i)$ points, calculated using the approximations given in the special Appendix C, was best-fitted. In fact, now it can be argued that this curve represents the so-called pseudorelaxation modulus, $E(t)$, because, as analyzed in detail in Appendix C, the algorithm developed in this way is valid only for initial loading times t_i greater than about ≈ 0.20 s and not for the "instantaneous" loading time $t_i \geq 10^{-10}$, which are the minimal mechanical relaxation times for a material estimated from other relaxation phenomena such as magnetic and dielectric.[15]

It must be stated that the previously described method, apart from the others, depends on the "extrapolation-to-zero" technique. This technique is widely applied for many cases and, despite the degree of uncertainty it includes, is the only approachable way. It must be pointed out that this "zero"-time approach is more direct and is achieved with better precision through the use of the virtual modulus than it would be through the use of the apparent modulus. In this sense, the approach through the use of the apparent modulus would require an extrapolation to zero for every given loading time and then a new extrapolation to zero through a curve of extrapolation points versus loading times.

There are some "crude criteria" to control the aforementioned results. In this sense, one is to check the "memory" of the final curve, that is, whether the calculated final result shown in Figure 6 "retains" some of the general characteristics or trends of the "initial" curves, that is, the $\tilde{E}(t)$, which are the ones which represent the apparent relaxation phenomenon. The first very simple criterion is to compare, for example, Figures 6 and 7 and to confirm, from similar shapes, the trend of decrease of the kinematical relaxation rate (intensity) when the loading time is reduced.

As is known and will be analyzed in more detail in Part II of this investigation, the relaxation phenomena are "governed" by certain general and empirical models, like the one of Kohlrausch–Williams–Watts (KWW) and the one of the "power law."[15] The first model is expressed through the modified best-fit linear relation: $\ln g(t) = a + bt^n$ $(0 < n \leq 1)$, and the second, also through the linear modified one: $\ln g(t) = \gamma + \beta \ln t$. Concerning the first relationship with the majority of polymers in the equilibrium state above $T_{g'}$ the parameter n is often found to be approximately $\frac{1}{2}$ for stage 1 of the relaxation process in the time range from zero to 1 h, whereas, concerning the second relationship, the parameter β is about $-\frac{1}{2}$.[15] Regarding PP, our calculation was made based on the relation $g(t) = \tilde{E}_i(t) - \tilde{E}_i(\infty)$, with $\tilde{E}_i(\infty) \neq 0$ and $\tilde{E}_i(0)/\tilde{E}_i(\infty) \cong \frac{1}{2}$ proved for many loading times t_i (for temperature of 25°C).

Thus, now according to that mentioned above, a second crude criterion will serve as a measure of comparison of the correlation factors r^2 from the best-fit procedure in these two models of the apparent modulus $\tilde{E}(t)$ and the pseudomodulus $E(t)$. This appears in Figures 8 and 9 and in Figures 10 and 11, where the best fit of these two moduli in the power-law and KWW models, respectively, is given. Here,

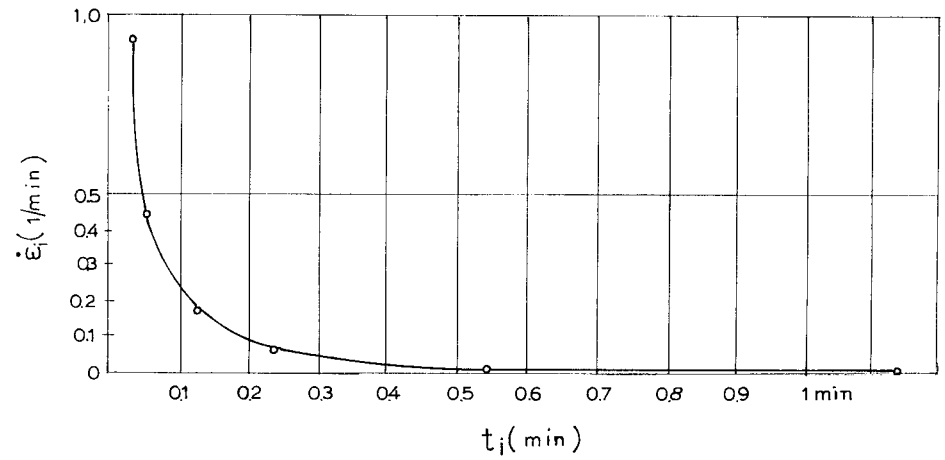

Figure 7 Strain rates versus loading times (for a given constant load).

the very good response of the apparent modulus to both models can be observed, but, at the same time, also the nonsatisfactory response of the calculated pseudomodulus mainly to the KWW model. The reason for this could be the fact that the virtual modulus itself has a relatively low correlation factor in both models, as it appears in Figures 12 and 13. However, we can also observe that, from the two models, the power-law model generally better approximates the three moduli.

As a third criterion, we can take advantage of the behavior of the three moduli as to the relaxation spectrum $H(\tau)$, which can be determined with some approximation through the "zeroth" approach of Alfrey[14]:

$$H(\tau) = \left.\frac{dE(t)}{d \ln t}\right|_{t=\tau} \tag{15}$$

The results of best fit for this case are given in Figures 14–16. From these figures, the very good approximation of the apparent modulus in Tobolsky's box-dis-

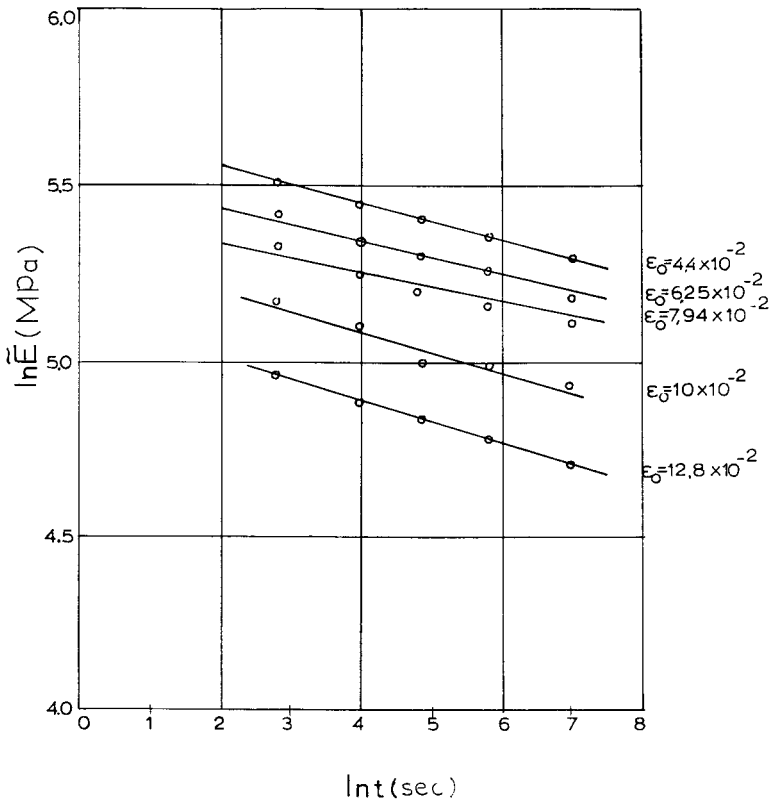

Figure 8 Linear regression (best-fit) curve of the apparent modulus for the power-law evidence (for strain rate $\approx 10^{-2}$/s).

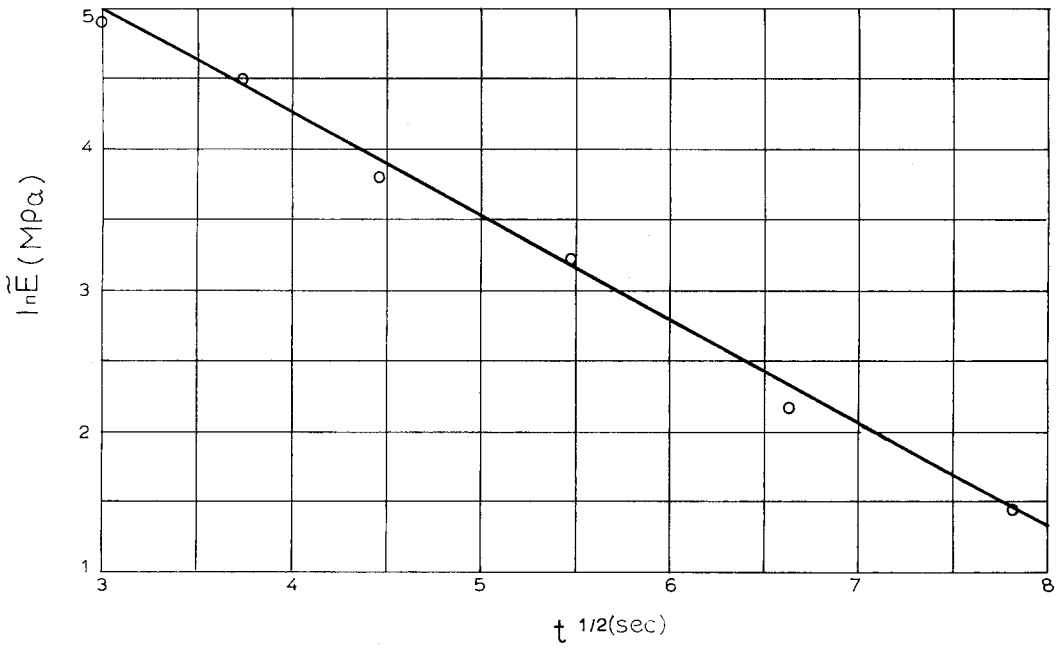

Figure 9 Linear regression (best-fit) curve of the apparent modulus for the KWW model evidence (for strain rate $\approx 10^{-2}$/s and initial strain $\varepsilon_0 \approx 12 \times 10^{-2}$).

tribution spectrum is observed and also the declination of the two other moduli $E(t)$ and $\bar{E}(t)$ from this given box distribution. Especially for the $E(t)$ modulus, we can assume that the relaxation spectrum separates into two linear ranges, that is, into two box-distributions, as can be distinguished in Figure 15.

From the above, the relative "memory loss" of the calculated pseudomodulus $E(t)$ in relation with the apparent $\tilde{E}(t)$ becomes evident, whose behavior, as to the points that we examined above, we consider as "right," and, consequently, it constitutes a reference basis for the validity check of the proposed modeling by the virtual modulus.

This memory loss must be further investigated in the behavior of the virtual modulus in Figures 12 and 16, from where nonlinear behavior is observed, that is, the beginning of a declination from the respective linearized models for reference strain ε_0 between 1

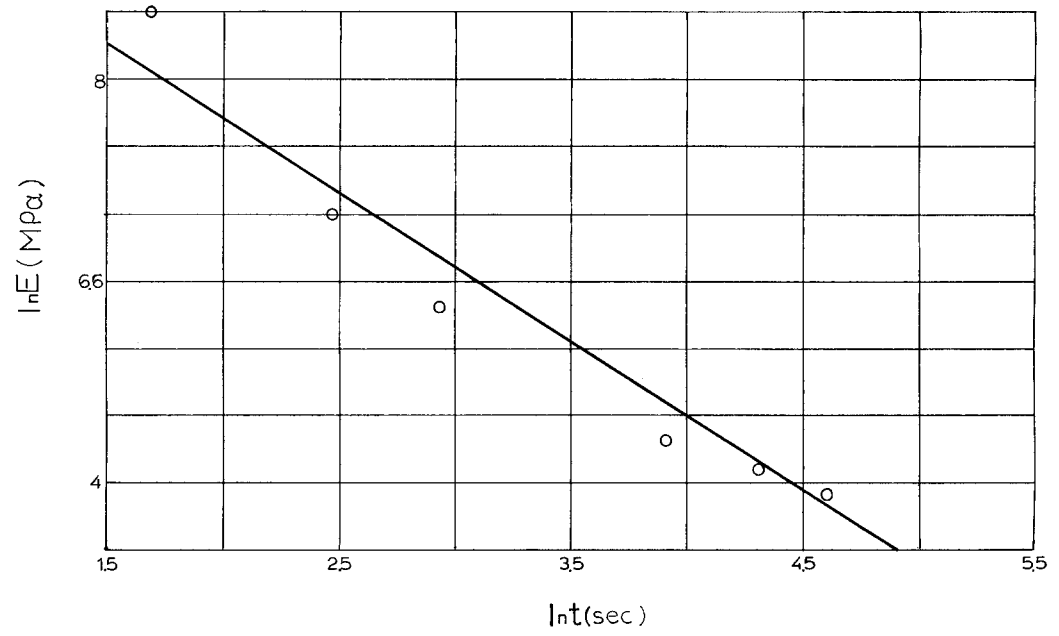

Figure 10 Linear regression (best-fit) curve of the calculated pseudomodulus for the power-law model evidence (from Fig. 6).

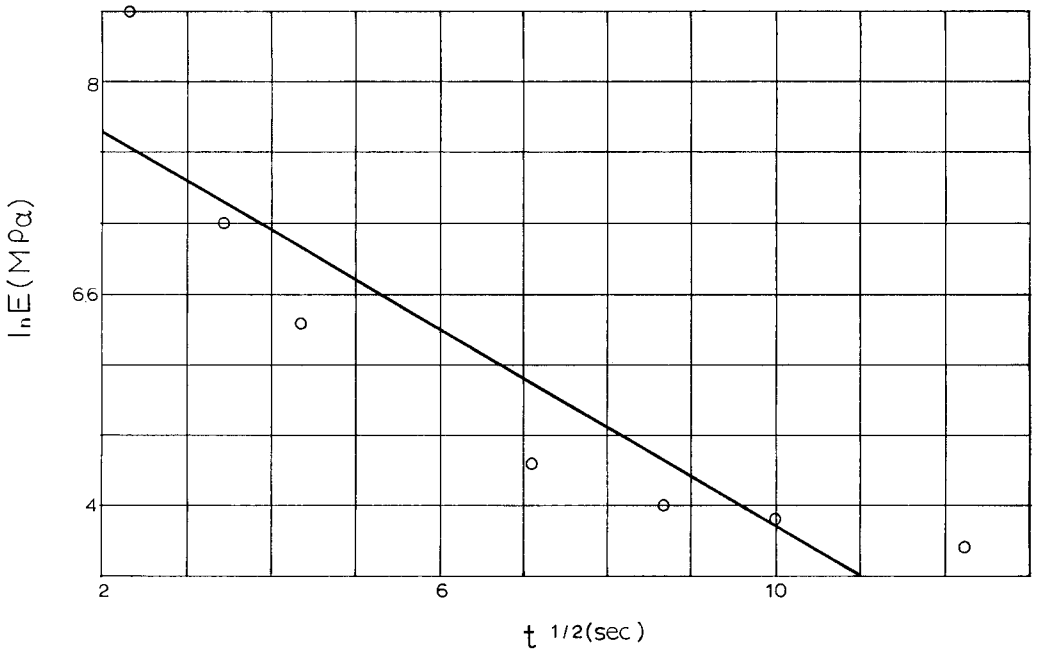

Figure 11 Linear regression (best-fit) curve of the calculated pseudomodulus for the KWW model evidence (from Fig. 6).

and 2%. Thus, it becomes clear that, through the virtual modulus, over about 2% strain, nonlinear viscoelastic effects are entering which decrease the approximation of the calculated pseudomodulus in relation to the real modulus.

As a fourth criterion, we can evaluate the fact that all the moduli for large experimental observation times and for a given initial strain should converge to one value. This fact is explained in more detail in Appendix B, from where it results that the general relationship $\bar{E}(t \to \infty) \cong E(t \to \infty) \cong \tilde{E}(t \to \infty)$ must be valid. Since the relaxation rate for iPP is very sensitive to the temperature, the experimental evidence of the above criterion should be examined. Taking into consideration all these, the related experiments showed that, for the initial strain of $\approx$1% and for times $t > 150$

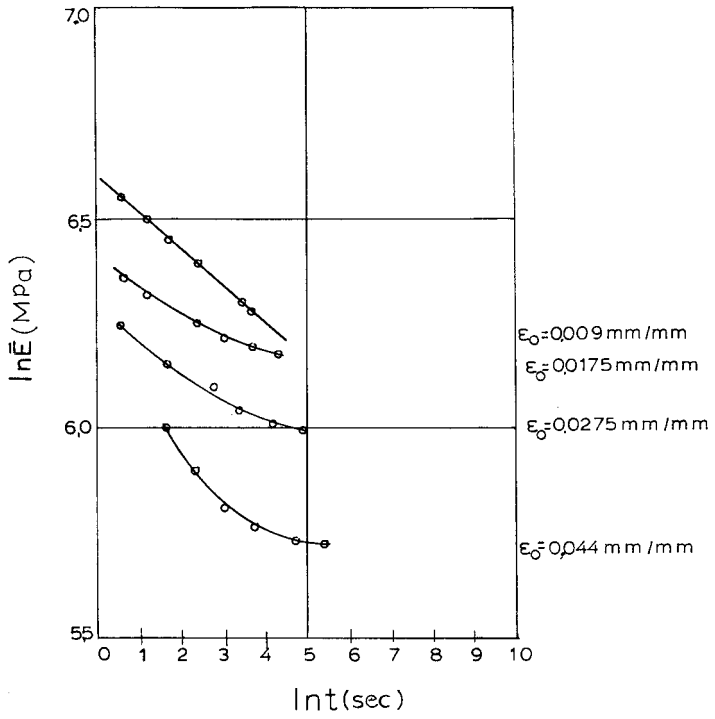

Figure 12 Linear regression (best-fit) curve of the virtual modulus for the power-law evidence for several reference strains.

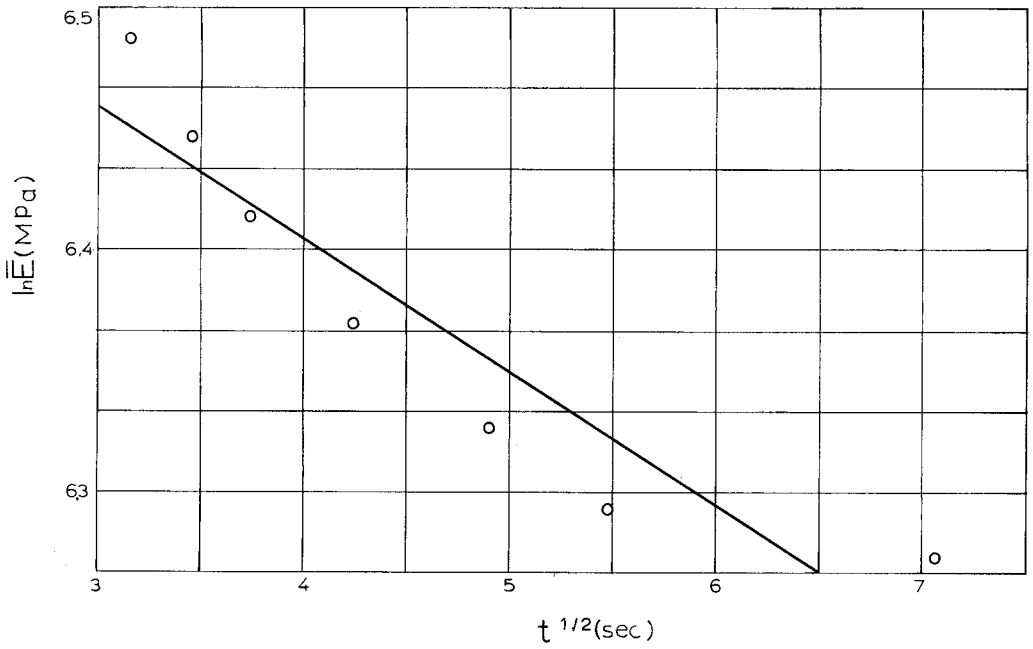

Figure 13 Linear regression (best-fit) curve of the virtual modulus for the KWW model evidence and for reference strain $\varepsilon_0 \approx 1\%$.

s, the three moduli tend to converge to the approximate value of 550 ± 50 MPa (see Figs. 5 and 6).

CONCLUSIONS

In this article, an effort was made to introduce, in a "modus operandi" way, a certain operational mode and parameter to characterize more effectively, through a profound study, the linear and nonlinear viscoelastic behavior of polymers using the example of iPP.

Depending on the method used and its corresponding parameter, this effort has shown the following:

(a) Using the virtual relaxation modulus and an adequate algorithmic approach, we obtained a

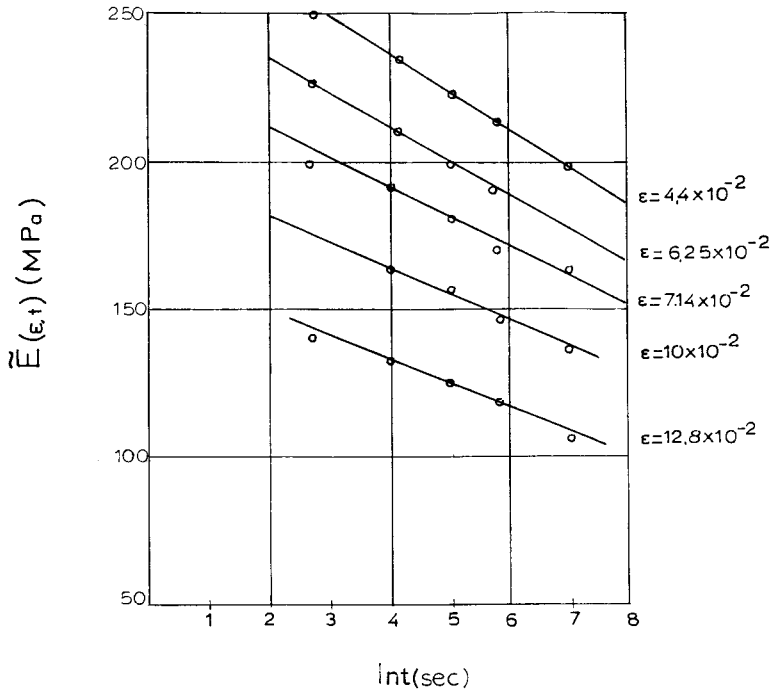

Figure 14 Spectral box-distribution evidence for the apparent modulus (for strain rate $\approx 10^{-2}$/s).

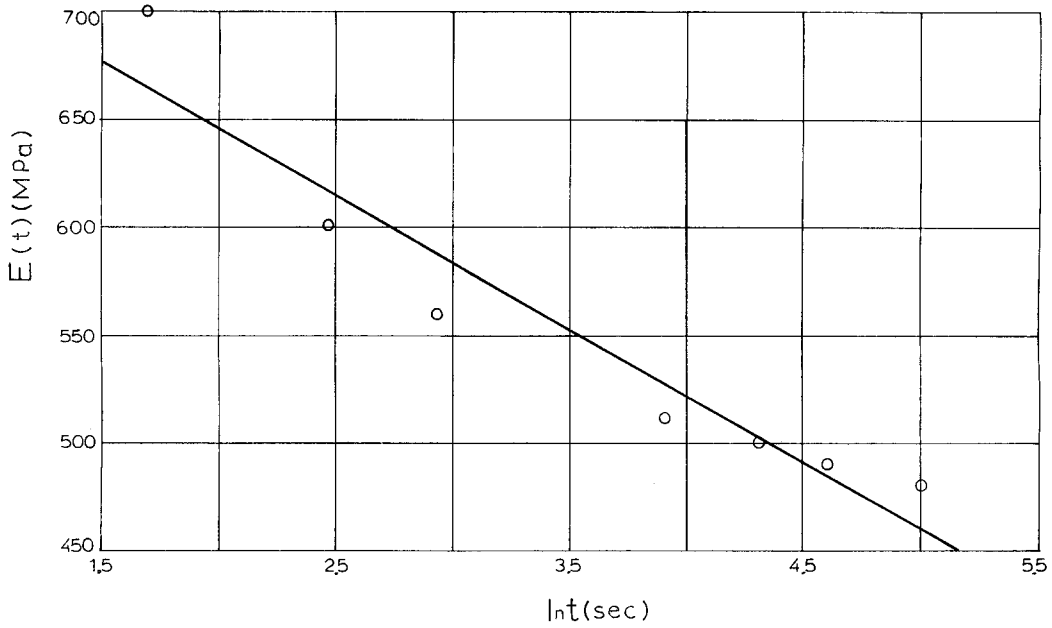

Figure 15 Spectral box-distribution evidence for the calculated pseudomodulus.

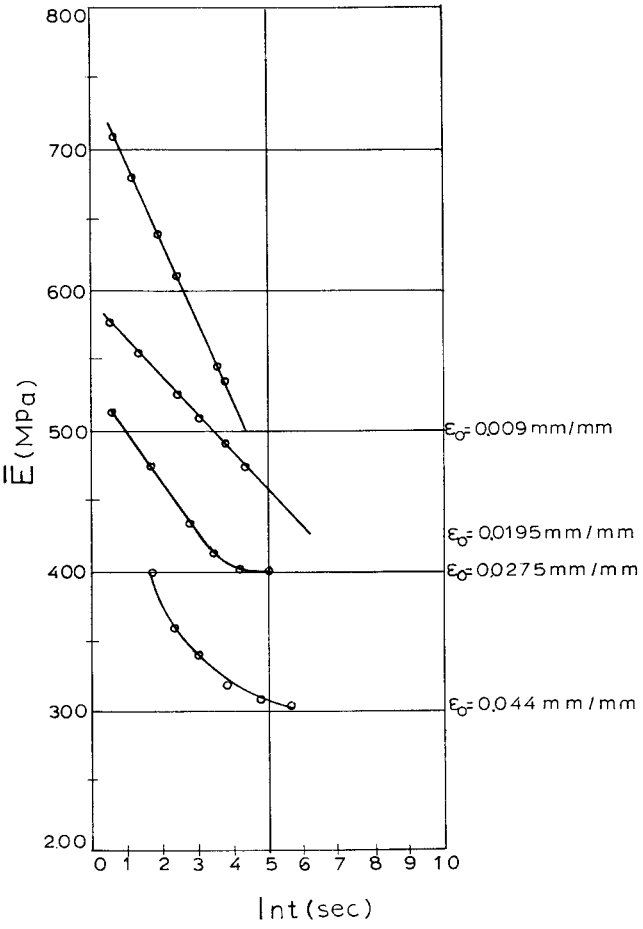

Figure 16 Spectral box-distribution evidence for the virtual modulus (for different strains).

pseudomodulus, which, under certain conditions, gives satisfactory results for the approximation of the real relaxation modulus for loading times down to $\frac{1}{5}$ s—something which is not feasible through experiments, due to the known phenomena of a machine's inertial effects, etc. At first instance, this pseudomodulus can be used as a "simulation" modulus of the "real" relaxation modulus, based on experimental data. Consequently, for the first instance, the practical meaning of this operational mode (parameter) is more academic rather than for broad use.

(b) Having this simulation as an operational tool, several polymeric materials can be compared with each other more effectively, since, at least as the first results show, this pseudomodulus seems to have larger experimental evidence sensitivity than has the apparent modulus.

(c) Taking into consideration the simplicity of the theoretical modeling, we can characterize the results as quite satisfactory and also encouraging for further studies and comparisons with other polymeric materials.

APPENDIX A: ABOUT THE INEQUALITY RELATION $\bar{E}(t) \geq E(t)$

A semiempirical distribution of the relaxation time spectrum $H(\tau)$ is given in the schematic in Figure A.1,, in a double-logarithmic scale, which is valid with a crude approximation for many polymers such as crystalline nylon-6 and methacrylate.[14] Therefore, there are four general distribution zones: from $\tau = \delta_0 > 0$ to $\tau = \delta_4' \gg 0$. The minimum relaxation time of the

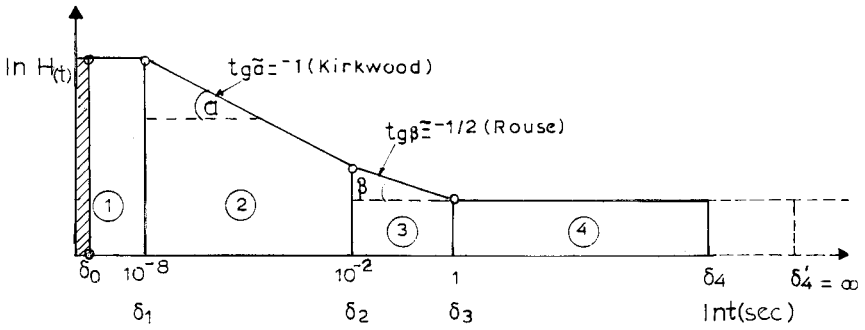

Figure A.1 Schematic spectral distribution zones of the relaxation times for PP.

molecules of a material according to solid polymer physics is not at "absolute zero," but is of the order of 10^{-10} s, which represents the easiest rotation of a group of CH_3 molecules. So, we have $\tau_{\min} \geq \delta_0 = 10^{-10}$ s (ref. 15).

Taking into consideration Figure 17, the general forms of the four distribution zones are as follows:

1. $10^{-10} \leq \tau \leq 10^{-8}$, $\ln H_1(\tau) = K_1 = \text{const}$ (box-distribution)
2. $10^{-8} \leq \tau \leq 10^{-2}$, $\ln H_2(\tau) = K_2 \ln \tau + K_2'$, where $K_2 = -1$ (Kirkwood model)
3. $10^{-2} \leq \tau \leq 10^{0} = 1$, $\ln H_3(\tau) = K_3 \ln \tau + K_3'$, where $K_3 = -\frac{1}{2}$ (Rouse model)
4. $\tau > 1$, $\ln H_4(\tau) = K_4$, where $K_4 = \text{const}$ (Tobolsky's box-distribution).

From the relation of the kinematic relaxation,

$$\sigma(t) = \dot{\varepsilon} \cdot \int_0^t \int_{-\infty}^{+\infty} H(\tau) e^{-t'/\tau}\, d \ln \tau\, dt' \qquad \text{(A.1)}$$

the following equation is obtained:

$$\frac{\sigma(t)}{\varepsilon} = \frac{1}{t} \int_0^t \int_0^\infty E(\tau) e^{-t'/\tau}\, d\tau\, dt' = \frac{1}{t} \int_0^\infty \times \tau E(\tau)[1 - e^{-t/\tau}]\, d\tau = \frac{1}{t} \int_0^t E(t')\, dt' = \bar{E}(t)$$

$$= \text{"virtual relaxation modulus"}$$

Therefore, it has to be shown for which observation times "t" the following inequality is valid:

$$\frac{1}{t} \int_0^\infty H(\tau)[1 - e^{-t/\tau}]\, d\tau \geq \int_0^\infty E(\tau) e^{-t/\tau}\, d\tau \qquad \text{(A.2)}$$

where

$$\int_0^\infty (\quad) = \int_{\delta_0}^{\delta_1} + \int_{\delta_1}^{\delta_2} + \int_{\delta_2}^{\delta_3} + \int_{\delta_3}^{\delta_4} + \cdots$$

1. For the first zone, we have

$$H_1(\tau) = e^{k_1} = \text{const} = \bar{K}_1$$
$$E(\tau) = \bar{K}_1/\tau$$

by substituting in eq. (A.2):

$$\int_{\delta_0}^{\delta_1} \bar{K}_1\, d\tau \geq t \int_{\delta_0}^{\delta_1} \frac{\bar{K}_1}{\tau} e^{-t/\tau}\, d\tau + \int_{\delta_0}^{\delta_1} \bar{K}_1 e^{-t/\tau}\, d\tau \qquad \text{(A.3)}$$

Taking that $1/\tau = z$,

$$\int_{\delta_0}^{\delta_1} e^{-t/\tau}\, d\tau = \left[\frac{e^{-t\cdot z}}{z}\right]_{1/\delta_0}^{1/\delta_1} + t \int_{1/\delta_0}^{1/\delta_1} \frac{e^{-t\cdot z}}{z}\, dz \qquad \text{(A.3a)}$$

and

$$\int_{\delta_0}^{\delta_1} \frac{1}{\tau} e^{-t/\tau}\, d\tau = -\int_{1/\delta_0}^{1/\delta_1} \frac{1}{z} e^{-t\cdot z}\, dz \qquad \text{(A.3b)}$$

In this way, the following inequality is obtained:

$$[\tau]_{\delta_0}^{\delta_1} > \left[\frac{e^{-t\cdot z}}{z}\right]_{1/\delta_0}^{1/\delta_1} = [e^{-t/\tau}\tau]_{\delta_0}^{\delta_1} \qquad \text{(A.4)}$$

and, finally,

$$[\delta_1 - \delta_0] \geq \delta_1 e^{-t/\delta_1} - \delta_0 e^{-t/\delta_0} \qquad \text{(A.5)}$$

Using some algebra, it can be shown that, for the given time $\delta_0 = 10^{-10}$ s and $\delta_1 = 10^{-8}$ s, the above relation is valid for all observation times $t \geq 0$ s.

2. For the second distribution zone (Kirkwood model), we have

$$H(\tau) = \tau^{-1}\bar{K}_2 \quad \text{and} \quad E(\tau) = \tau^{-2}\bar{K}_2, \quad \text{with} \quad K_2' = \ln \bar{K}_2$$

and by substituting in eq. (2), we have

$$\int_{\delta_1}^{\delta_2} \frac{1}{\tau}\, d\tau > t \int_{\delta_1}^{\delta_2} \frac{1}{\tau^2}\, e^{-t/\tau}\, d\tau + \int_{\delta_1}^{\delta_2} \frac{1}{\tau}\, e^{-t/\tau}\, d\tau \tag{A.6}$$

Using the transformations $1/\tau = z$, $d\tau = -(1/z^2)\, dz$, and $dz = (-d\tau)/\tau^2$,

$$\int_{\delta_1}^{\delta_2} \frac{1}{\tau}\, e^{-t/\tau}\, d\tau = -\int_{1/\delta_1}^{1/\delta_2} \frac{1}{z}\, e^{-t\cdot z}\, dz = \left\{ [\ln z]_{1/\delta_1}^{1/\delta_2} + \left[\sum_{n=1}^{\infty} \frac{(-tz)^n}{n \cdot n!} \right]_{1/\delta_1}^{1/\delta_2} \right\} (-1) \tag{A.6a}$$

$$\int_{\delta_1}^{\delta_2} \frac{1}{\tau^2}\, e^{-t/\tau}\, d\tau = -\int_{1/\delta_1}^{1/\delta_2} e^{-t\cdot z}\, dz = \frac{1}{t}\, [e^{-t\cdot z}]_{1/\delta_1}^{1/\delta_2} = \frac{1}{t}\, [e^{-t/\delta_2} - e^{-t/\delta_1}] \tag{A.6b}$$

$$\int_{\delta_1}^{\delta_2} \frac{1}{\tau}\, d\tau = \ln\, \tau]_{\delta_1}^{\delta_2} = \ln(\delta_2/\delta_1), \quad (\delta_2 > \delta_1)$$

After some simplifications, it remains to be shown that

$$e^{-t/\delta_1} - e^{-t/\delta_2} \geq \sum_{n=1}^{\infty} [(-t/\delta_1)^n - (-t/\delta_2)^n]\, \frac{1}{nn!} \tag{A.7}$$

where, by using Taylor's expansion, we obtain

$$\sum_{n=1}^{\infty} [(-t/\delta_1)^n - (-t/\delta_2)^n]\, \frac{1}{n} \geq \sum_{n=1}^{\infty} [(-t/\delta_1)^n - (-t/\delta_2)^n]\, \frac{1}{nn!} \tag{A.8}$$

By defining $t/\delta_1 = x$, $t/\delta_2 = y$, $(1/n!)(x^n - y^n) = \Delta_n$, and $\Delta_n - \Delta_n(1/n) = \bar{\Delta}_n$, where $x \geq y$, because of $\delta_2 \geq \delta_1$, the relation (A.8) is modified as the following:

$$\sum_{n=1}^{\infty} (-1)^n \bar{\Delta}_n \geq 0 \tag{A.9}$$

This inequality is valid if it can be shown that $\bar{\Delta}_{2n} \geq \bar{\Delta}_{2n-1}$, which means that the following inequality must also be valid:

$$\Delta_{2n}\left(1 - \frac{1}{(2n)!}\right) \geq \Delta_{2n-1}\left(1 - \frac{1}{(2n-1)!}\right) \tag{A.10}$$

This means that we must have

$$\frac{\Delta_{2n}}{\Delta_{2n-1}} = \frac{(2n-1)!x\left[1 - \left(\frac{y}{x}\right)^{2n}\right]}{2n!1 - \left(\frac{y}{x}\right)^{2n-1}} \geq \frac{1 - \frac{1}{(2n-1)!}}{1 - \frac{1}{2n!}} \tag{A.11}$$

Taking now the limit $n \to \infty$, we obtain from (A.11) the solution $x \geq 1$, which by $t/\delta_1 = x$ becomes $t \geq 10^{-8}$ s.

3. For the Rouse-type distribution, we have

$$H(\tau) = \tau^{-1/2}\bar{K}_3 \quad \text{and} \quad E(\tau) = \tau^{-3/2}\bar{K}_3, \quad \text{with} \quad K_3' = \ln \bar{K}_3 \tag{A.12}$$

Substituting in relation (A.2),

$$\int_{\delta_2}^{\delta_3} \frac{1}{\sqrt{\tau}}\, d\tau \geq t \int_{\delta_2}^{\delta_3} \frac{1}{\tau^{3/2}}\, e^{-t/\tau}\, d\tau + \int_{\delta_2}^{\delta_3} \frac{1}{\sqrt{\tau}}\, e^{-t/r}\, d\tau \tag{A.13}$$

Using the following transformations of the variables,

$$z = \frac{1}{\tau}, \quad dz = -\frac{d\tau}{\tau^2}, \quad d\tau = -\frac{dz}{z^2} \tag{A.13a}$$

$$\int_{\delta_2}^{\delta_3} \frac{1}{\sqrt{\tau}}\, e^{-t/\tau}\, d\tau = -\int_{1/\delta_2}^{1/\delta_3} \frac{1}{z^{3/2}}\, e^{-t\cdot z}\, dz = \frac{1}{1 - 3/2} \left\{ \left[-\frac{e^{-tz}}{z^{1/2}} \right]_{1/\delta_2}^{1/\delta_3} - t \int_{1/\delta_2}^{1/\delta_3} \frac{e^{-t\cdot z}}{\sqrt{z}}\, dz \right\} \tag{A.13b}$$

$$\int_{1/\delta_2}^{1/\delta_3} \frac{e^{-t\cdot z}}{\sqrt{z}}\, dz = 2 \int_{\sqrt{1/\delta_3}}^{\sqrt{1/\delta_2}} e^{-tq^2}\, dq, \quad \text{for } \sqrt{z} = q \quad \text{and} \tag{A.13c}$$

$$\int_{\delta_2}^{\delta_3} \frac{1}{\tau^{3/2}}\, e^{-t/\tau}\, d\tau = (-2) \int_{\sqrt{1/\delta_3}}^{\sqrt{1/\delta_2}} e^{-tq^2}\, dq, \quad \text{with } \frac{1}{\sqrt{\tau}} = q \tag{A.13d}$$

Then, relation (A.13) is modified:

$$2 \cdot \delta_2[\sqrt{\tau}]_{\delta_2}^{\delta_3} \geq (-2)t \int_{\sqrt{1/\delta_2}}^{\sqrt{1/\delta_3}} e^{-tq^2}\, dq + [2e^{-t/\tau}\sqrt{\tau}]_{\delta_2}^{\delta_3} + 4t \int_{\sqrt{1/\delta_2}}^{\sqrt{1/\delta_3}} e^{-tq^2}\, dq \quad \text{(A.14)}$$

and after some simplifications,

$$\sqrt{\delta_3} - \sqrt{\delta_2} + t \int_{\sqrt{1/\delta_3}}^{\sqrt{1/\delta_2}} e^{-tq^2}\, dq \geq [\sqrt{\tau}e^{-t/\tau}]_{\delta_2}^{\delta_3} = \sqrt{\delta_3}\, e^{-t/\delta_3} - \sqrt{\delta_2}\, e^{-t/\delta_2} \quad \text{(A.15)}$$

where for $t = 0$, the following identity is obtained:

$$\sqrt{\delta_3} - \sqrt{\delta_2} \equiv \sqrt{\delta_3} - \sqrt{\delta_2} \quad \text{(A.15a)}$$

Since the integral in inequality (A.15) yields a positive contribution, because it has a positive value, this inequality would be even more valid if the inequality is valid:

$$\sqrt{\delta_3} - \sqrt{\delta_2} \geq \sqrt{\delta_3}\, e^{-t/\delta_3} - \sqrt{\delta_2}\, e^{-t/\delta_2} \quad \text{(A.15b)}$$

This inequality is similar to eq. (A.5) and, consequently, through similar algebraic calculation, we can prove easily that relationship (A.15b) is valid for all observation times $t \geq 0$ s.

4. For the last zone, the procedure is the same as that for the first zone, where it was proved that the inequality (A.2) is valid for all loading times $t \geq 0$ s.

It must be noted that the constant K_4 of the distribution of this last zone of the spectrum can be estimated by the "zeroth" Alfrey approximation eq. (15) in the text, through the experimental data of Figure 8. Also, it has to be noted that, from the above calculations, it can be deduced that the general basic inequality $\tilde{E}(t) \geq E(t)$ is not valid for all observation experimental times $t \geq 0$ but for specific time intervals depending on the distribution zone. In this sense, there is a common lower limit of an observation time for all zones, of the order of 10^{-8} s, which is, by far, the range of experimental time data for which the algorithmic modeling approach, concerning the existence of the virtual modulus, is valid (see Appendix C).

APPENDIX B: ABOUT THE INEQUALITY RELATION $\tilde{E}(t) \geq E(t)$

This topic is related to the influence of the loading time t_i, or the constant deformation rate $\dot{\varepsilon}_0$, on the mode of relaxation of a polymer under constant strain ε_0. So, for a given loading time t_i, the apparent stress $\tilde{\sigma}(t)$, which is observed after time $t \geq t_i$, is given by the following relation[12]:

$$\tilde{\sigma}(t) = \frac{\varepsilon_0}{t_i} \int_{t-t_i}^{t} \int_{-\infty}^{+\infty} [H(\tau)e^{-t'/\tau}] d \ln \tau\, dt'$$

which is modified to

$$\dot{\varepsilon}_0 \int_{t-t_i}^{t} E(t')\, dt' = \dot{\varepsilon}_0 \int_{-\infty}^{+\infty} \left[\int_{t-t_i}^{t} H(\tau)e^{-t'/\tau} \right] dt'\, d \ln \tau$$

$$= \dot{\varepsilon}_0 \int_{-\infty}^{+\infty} [-\tau H(\tau)e^{-t'/\tau}]_{t-t_i}^{t} d \ln \tau$$

$$= \dot{\varepsilon}_0 \int_{-\infty}^{+\infty} \tau H(\tau)[-e^{-t/\tau} + e^{-(t-t_i/\tau)}]\, d \ln \tau$$

$$= \dot{\varepsilon}_0 \int_{-\infty}^{+\infty} H(\tau)\tau e^{-t/\tau} \times [(e^{-t_i/t})^{-t/\tau} - 1]\, d \ln \tau \quad \text{(B.2)}$$

By assuming that $t_i/t \ll 1$, we have $e^{-t_i}/t \cong 1 - t_i/t$ and $(1 - t_i/t)^{-t/\tau} = 1 + t_i/\tau$ and the following simpler relation is obtained:

$$\tilde{\sigma}(t) \cong \frac{\varepsilon_0}{t_i} \int_{-\infty}^{+\infty} H(\tau)\tau[e^{-t/\tau}(1 + t_i/\tau) - e^{-t/\tau}]\, d \ln \tau$$

$$= \varepsilon_0 \int_{-\infty}^{+\infty} H(\tau)e^{-t/\tau}\, d \ln \tau = \varepsilon_0 E(t) = \sigma(t) \quad \text{(B.3)}$$

This means that, for $t_i \ll t$, the "apparent" stress is becoming equal with the "ideal" stress. The same is valid for the corresponding relaxation moduli, that is, $\tilde{E}(t) = E(t)$. Struik[16] proved that, for $t_i/t \cong \frac{1}{10}$, the "apparent" modulus can be considered equal to the "ideal" (real) one. The above are valid considering the linear theory of viscoelasticity. For a nonlinear behavior, for these moduli to become equal, longer observation times are needed ($t > 10t_i$).

Now, for a quasistatic loading where $t_i \to t$, and taking a step-function approach as $e^{-t/\tau} = 0$ for $\tau \ll t$ and $e^{-t/\tau} = 1$ for $\tau \gg t$, we obtain from relation (B.2)

$$\tilde{\sigma}(t) \to 0 \quad \text{(B.4)}$$

In the text, it was shown that the virtual modulus is the result of a kinematic relaxation and, thus, for a quasi-static loading, that is, for $t \to t_i$ and using rela-

tion (B.4), it can be assumed that $\bar{E}(t_i) \cong \tilde{E}(t) \cong E(t) \rightarrow 0$. This means that all the relaxation moduli are tending to become identical for (very) long experimental observation times. The above-mentioned phenomena are better shown in the schematic of Figure 1.

APPENDIX C: ALGORITHMIC APPROACH OF THE "REAL" MODULUS $E(t)$ BY THE "VIRTUAL" RELAXATION MODULUS $\bar{E}(t)$

The following differential equation is to be solved:

$$\boxed{\dot{\varphi}(t) + \varphi(t)P(t) = Q(t)} \tag{C.1}$$

where

$$\varphi(t) = E(t), \quad P(t) = \frac{\dot{\bar{\psi}}(t) - 1}{\bar{\psi}(t)}, \quad Q(t) = \frac{\dot{f}(t)}{\bar{\psi}(t)}$$

and $f(t) = \chi(t)\bar{\psi}(t) - \bar{I}(t)$, where $\chi(t) = \bar{E}(t)$, $\bar{I}(t) = \int_0^t \bar{E}(t')dt'$, and $\bar{\psi}(t) = t[1 - \frac{1}{2}\psi(t)]$.

The "closed"-form solution of the differential eq. (C.1) is

$$E(t) = \varphi(t) = e^{-\int_0^t P(t')dt'}\left[\int_0^t Q(t')\, e^{\int_0^{t'} P(x)dx}\, dt' + c\right] \tag{C.2}$$

where $c = \varphi(t = 0) = E(t = 0)$.

First, the following integral is determined:

$$\int_0^t P(t')\, dt' = \int_0^t \frac{\dot{\bar{\psi}}(t')}{\bar{\psi}(t')}\, dt' - \int_0^t \frac{dt'}{\bar{\psi}(t')} \tag{C.3}$$

To simplify the parabola $\psi(t)$, it was possible to take an approximation with the line $\psi(t) \cong 1 + 0,2t$, which is good for the time interval $0 \leq t \leq 3$ min. Thus, the function

$$\bar{\psi}(t) = t\left(1 - \frac{1}{2\psi(t)}\right)$$

is obtained and the integral (C.3) is modified:

$$\int_0^t P(t')\, dt' = [\ln \bar{\psi}(t)]_0^t - \int_0^t \frac{\psi(t')\, dt'}{t'(\psi(t') - \frac{1}{2})} \tag{C.4}$$

From integral tables, we have

$$\int_0^t \frac{\psi(t')\, dt'}{t'(\psi(t') - \frac{1}{2})} = \ln \frac{t^2}{0.2t + \frac{1}{2}} \tag{C.4a}$$

Hence, the following function is obtained:

$$F_2(t) = e^{-\int_0^t P(t')dt'} = \frac{1}{\bar{\psi}(t)} \frac{t^2}{0,2t + \frac{1}{2}} = \frac{0.2t^2 + t}{0,2^2t^2 + 0,2t + \frac{1}{4}} \tag{C.5}$$

We also find

$$F_1(t') = e^{\int_0^{t'} P(x)dx} = \bar{\psi}(t') \frac{0.2t' + \frac{1}{2}}{t'^2} \tag{C.5a}$$

and

$$I_k(t) = \int_{\delta_k}^t Q(t')F_1(t') = \int_{\delta_k}^t f(t') \frac{at' + \frac{1}{2}}{t'^2}\, dt' = I(t, \delta_K) \tag{C.5b}$$

It is obvious that $\lim_{\delta_k \rightarrow 0} I_k(t) \rightarrow \infty$ and, therefore, for this case, the problem is vague and complicated. Nevertheless, from the polymer physics,[15] it is known that the minimal relaxation time is approximately 10^{-10} s (not "absolute null") and, therefore, we have $\delta_k \cong 10^{-10}$ s.

Consequently, a basic theoretical condition in order that the problem have a solution is

$$I_k(t \rightarrow \infty) = \lambda_k = \text{const} \tag{C.6}$$

This was clearly shown in the PC charts, where the integral $I_k(t)$ was stabilized into a certain value for as long as t is increasing and for a certain given value δ_k.

Another basic experimental condition which must also be kept is

$$E(t \rightarrow \infty) = \lim_{t \rightarrow \infty} F_2(t)[I_k(t) + c] \cong E_\infty \cong \text{const} \tag{C.7}$$

where the constant for iPP is $E_\infty \cong E(0)/2$ for a temperature of 25°C and which is almost independent of the strain rate. The constant c is is determined from the relation $\bar{E}(0) = E(0) = c$, based on the values arising from the extrapolation of the corresponding best-fit function in Figure 6 for $t = 0$, from which we obtain $C \cong 1200$ MPa. Furthermore, we can also approach the equation $F_2(t) \cong 5$ for $t \rightarrow \infty$ or at least for conveniently long times. Therefore, using the values elicited from above, the condition (C.7) becomes

$$\lim_{t \rightarrow \infty} 5(\lambda_k + 1200) = 600 \tag{C.7a}$$

stating that, for long times, we must have $\lambda_k \cong -1080$. This means that, through the conditions (C.6) and

(C.5b), we must find a "suitable" initial loading time or kinematical relaxation time "δk" to satisfy them. In this way, it was found that this is valid for $\delta_k \cong 20 \times 10^{-2}$ to 25×10^{-2} s. Consequently, the model developed in this Appendix does not "operate" for initial relaxation times (loading times), which are less than about one-fifth of a second.

To have a more general picture regarding the practical efficiency of this model algorithm, we can make the following estimations: For a specimen with a "moderate" length, with $l_0 = 100$ mm, and for a machine with "fast-efficient" loading and crosshead speeds of 1 mm/s, for which there are no deficiencies due to the machine's inertial effects or to transitional speeds,[13] and for a "practical" linear viscoelastic deformation $\cong 1\%$, we take a relevant "reference" loading time of $t \cong 1$ s. Considering this time as a reference measure for the performance of such a reference method, it appears that our method is "not so efficient," as we achieved "only" a $\frac{1}{5}$ to $\frac{1}{4}$ reduction of the "reference" loading time. But, we should mention that, for the calculation of the "pseudo-real" curve $E(t)$, we used the data of the initial $\bar{E}(0)$ and $E(0)$ moduli, calculated through the extrapolation of the "best-fit" curve, which has a relatively high degree of approximation ($r^2 \cong 0.98$). Therefore, we think that the so-determined pseudomodulus must be much closer to the real one than are the ones determined from an experiment with a loading time of approximately 1 s or greater.

Regarding the choice of the $\chi(t) = \bar{E}(t)$ and $I(t)$ functions, we should mention the following: With the help of best fit, we found that, in general, $\bar{E}_i(t) = \beta e^{-at} + \alpha$, with a correlation factor $r^2 \cong 0.98$. Also, from very simple planimetric measurements, it was shown that

$$\frac{(\text{Area value})}{\beta \int_0^t (\varepsilon^{-at'} + \alpha)\, dt'} \cong 1 \pm 5\%$$

thus arriving at $I(t) = \int_0^t \bar{E}(t)\, dt$ with a good approximation.

As the $f(t)$ equation has been approached through experimental data with the help of best-fit, various "uncontrollable" great errors would intrude by the equation's differentiation [i.e., for $\dot{f}(t)$], if $f(t)$ would present maximum–minimum value points. But the course of $f(t)$ for $t > 0$ times does not present such points and, therefore, there are no such errors.

References

1. Duffo, P.; Monasse, B.; Maudin, J.; Sell, C.; Dahonn, A. J Mater Sci 1995, 30, 701.
2. Reinshagen, J. H.; Dunlap, R. W. J Mater Sci 1975, 19, 1037.
3. Shinozaki, D. M.; Klausner, A. J Mater Sci 1991, 26, 5865.
4. Sween, J.; Ward, J. M. J Mater Sci 1990, 25, 697.
5. Goble, D. L.; Wolf, E. G. J Mater Sci 1993, 28, 5986.
6. Kubat, J.; Rigdahl, M.; Selden, R. Eng Appl Polym Sci 1976, 20, 2799.
7. Hedworth, J.; Stowell, M. Y. J Mater Sci 1971, 6, 1061.
8. Chandra, M.; Roy, S. K. Plastics Technologie Handbook; Marcel Dekker: New York, 1987.
9. Tobolsky, A. V. Properties and Structure of Polymers; Wiley: New York, 1960.
10. Martakis, N.; Niaounakis, M.; Pissimissis, D. J Appl Polym Sci 1994, 51, 313.
11. Wunderlich, B. In Macromolecular Physics: Crystal Melting; Academic Press: New York, 1980; Vol. 3, p 48.
12. Hedworth, J.; Stowell, M. J. J Mater Sci 1971, 6, 1061.
13. Kobayashi, A.; Ohtani, N. J Appl Polym Sci 1971, 15, 975.
14. Ferry, J. D. Viscoelastic Properties of Polymers; Wiley: New York, London, 1961.
15. Matsuoka, S. Relaxation Phenomena in Polymers; Hanser: Munich, Vienna, New York, Barcelona, 1992.
16. Struik, J. C. E. Physical Aging in Amorphous Polymers and Other Materials; Elsevier: Amsterdam, 1978.